ACS OMEGA

Article

Cite This: ACS Omega 2019, 4, 16906−16915

http://pubs.acs.org/journal/acsodf

A Comparative Computational Study of the Adsorption of TCNQ and F4-TCNQ on the Coinage Metal Surfaces

Roberto Otero,[†,‡] Rodolfo Miranda,[†,‡] and José M. Gallego*[,¶]

[†]Dep. de Física de la Materia Condensada, Universidad Autónoma de Madrid, Cantoblanco, 28049 Madrid, Spain

[‡]Instituto Madrileño de Estudios Avanzados en Nanociencia (IMDEA-Nanociencia), Cantoblanco, 28049 Madrid, Spain

[¶]Instituto de Ciencia de Materiales de Madrid, CSIC, Cantoblanco, 28049 Madrid, Spain

ABSTRACT: The adsorption of tetracyanoquinodimethane and of the closely related derivative tetrafluorotetracyanoquinodimethane on the (111) surfaces of the coinage metals, namely, copper, silver, and (unreconstructed) gold, has been studied by dispersion-corrected ab initio density functional theory calculations. In order to separate the molecule−substrate interaction from the effects of molecule−molecule interaction, only the isolated molecules are considered. The results show that, in this case, the strength of the interaction of both molecules with the surfaces decreases in the expected order Cu > Ag > Au. The total amount of charge transfer, however, behaves in a different way, being larger for Ag and smaller for Cu and Au. This trend can be explained by a combination of the differences in the work functions of the three metals and the amount of backdonation between the molecule and the metal.

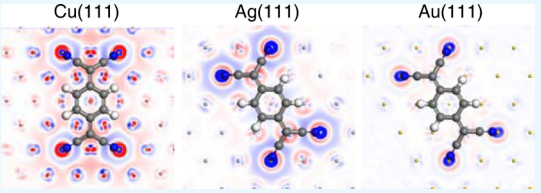

INTRODUCTION

Organic electronics has received an impressive boost in the last years, and organic electronic devices, like printed solar cells or flexible lights and displays, are starting to become part of our everyday life.[1−3] Being both a cause and a consequence of this rapid growth, the study of the electronic properties of organic compounds, in general, and of electron-acceptor or electron-donor species, in particular, as fundamental components of these devices, has concurrently been the subject of an increasing level of attention.[4,5] In particular, the interaction of an organic layer of electron-acceptor molecules with a metal surface has been extensively studied since it was soon realized that the performances of these devices strongly depend on the energy barriers at the metal−organic interfaces within[6−15] and it has become clear by now that the deposition of an organic molecule on a metal substrate can affect the structural and electronic properties of both the molecule and the metal surface,[15,16] thus modifying the injection energy barriers from the expected vacuum energy level alignment.

Since its first synthesis[17] and the subsequent report of a high electrical conductivity in some of its salts,[18−20] 7,7,8,8-tetracyanoquinodimethane (TCNQ) (Figure 1a) has assumed a very important role in these research studies. TCNQ is one of the strongest organic electron-acceptor molecules, with a high electron affinity (between 2.88 and 3.38 eV),[21−23] and able to form a large number of charge transfer complexes with metallic or organic donors,[24] some of which are superconductive at relatively high temperatures.[25] It is also a component of many molecule-based organic magnets[26] and participates in enzyme-based biosensors.[27] The derivative compound 2,3,5,6-tetrafluoro-7,7,8,8-tetracyanoquinodimethane (F4-TCNQ) (Figure 1b), obtained by the substitution of the peripherical hydrogen atoms with electronegative

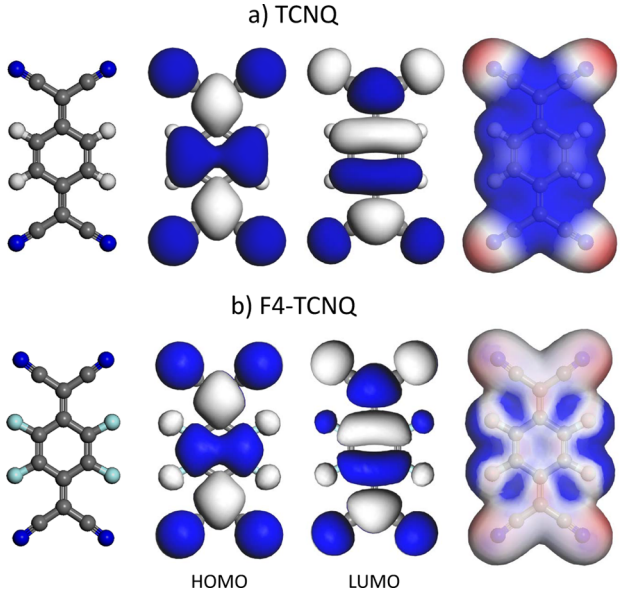

Figure 1. Calculated gas-phase conformations, HOMO and LUMO orbitals, and electronic isosurfaces for (a) TCNQ and (b) F4-TCNQ. The frontier orbital isosurfaces correspond to an electron density of 0.01 electrons/Å^3. The electronic isosurface represents a surface of points with the same total electron density (0.03 electrons/Å^3) colored according to the values of the electrostatic potential in every point.

Received: July 12, 2019
Accepted: September 11, 2019
Published: October 4, 2019

DOI: 10.1021/acsomega.9b02154
ACS Omega 2019, 4, 16906−16915

Table 1. Bond Lengths (in Å) of the Neutral TCNQ and F4-TCNQ Molecule ($TCNQ^0$ and $F4\text{-}TCNQ^0$) in the Anion ($TCNQ^{1-}$ and $F4\text{-}TCNQ^{1-}$) and Dianion ($TCNQ^{2-}$ and $F4\text{-}TCNQ^{2-}$) States and when Adsorbed on the Cu(111), Ag(111), and Au(111) Surfaces

bond length	$TCNQ^0$	$TCNQ^{1-}$	$TCNQ^{2-}$	TCNQ/Cu(111)	TCNQ/Ag(111)	TCNQ/Au(111)
B1	1.362	1.378	1.395	1.391	1.392	1.381
B2	1.440	1.425	1.415	1.410	1.413	1.421
B3	1.401	1.435	1.470	1.471	1.463	1.438
B4	1.423	1.414	1.406	1.395	1.399	1.407
B5	1.172	1.178	1.187	1.190	1.186	1.182
bond length	$F4\text{-}TCNQ^0$	$F4\text{-}TCNQ^{1-}$	$F4\text{-}TCNQ^{2-}$	F4-TCNQ/Cu(111)	F4-TCNQ/Ag(111)	F4-TCNQ/Au(111)
B1	1.366	1.378	1.392	1.369	1.389	1.384
B2	1.440	1.424	1.414	1.438	1.411	1.417
B3	1.400	1.430	1.460	1.402	1.458	1.443
B4	1.425	1.419	1.413	1.423	1.404	1.408
B5	1.171	1.175	1.182	1.172	1.184	1.182

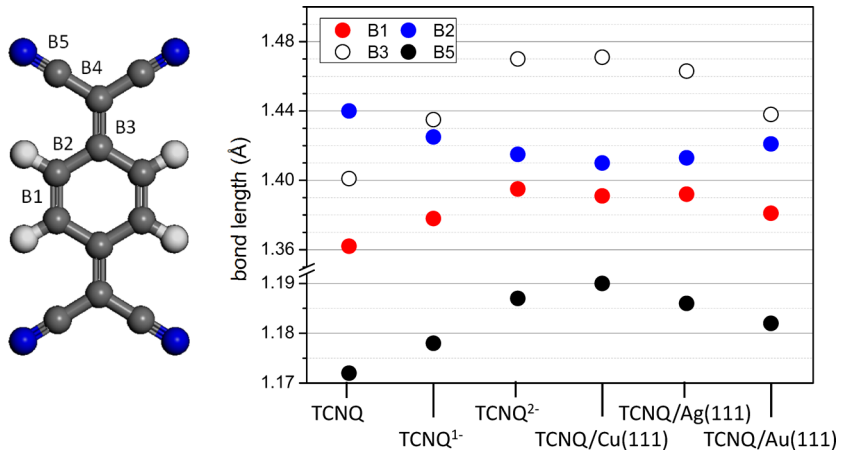

Figure 2. Lengths (in Å) of the B1, B2, B3, and B5 bonds of the TCNQ molecule in the neutral form, in the anion and dianion states, and when adsorbed on the Cu(111), Ag(111), and Au(111) surfaces.

fluorine atoms, shows an even greater acceptor behavior, with an electron affinity of 5.08−5.24 eV.[28] Both molecules have been routinely used to decrease the hole injection barrier at the metal−organic interface either by doping the hole transport layer or as an intermediate buffer layer between the hole transport layer and the metal anode.[29−32] Recently, it has also been shown that doping the electron injection layer with TCNQ[33] or inserting a TCNQ buffer layer between the electron transport layer and the metal cathode[34] can also improve the performance of organic light-emmiting devices.

The adsorption of TCNQ and F4-TCNQ on different metal surfaces has been the subject of many different experimental and theoretical studies.[16,31,35−56] From the early results, it was clear that both molecules adsorb flat on most metal surfaces, accepting negative charge from the substrate and causing an increase in the work function of the system. Maybe the only exception is the adsorption of TCNQ on the Au(111) surface. In here, a decrease of the work function has been experimentally measured,[44,55] and both theory and experiments seem to indicate that TCNQ is physisorbed on the Au(111) surface and there is no charge transfer between the molecule and the gold substrate.[39,43,52,55] In some cases, molecular distortion and/or surface reconstruction have also been reported.[16,38,40,46−48,51,53] Upon adsorption, the molecule has been claimed to adopt a bent geometry, with the cyano groups closer to the surface than the central carbon ring, while the metal atoms directly underneath the nitrogen atoms are slightly pulled outward the surface. More recently, however, this bending geometry has been questioned. In particular, for the TCNQ/Ag(111) system, a more planar molecular structure with the presence of substrate adatoms has been demonstrated.[56] Actually, besides TCNQ on Ag(111),[44,56,57] the participation of adatoms in the room temperature assembly of TCNQ and F4-TCNQ on Au(111) has also been suggested.[44,45,55−58] To what extent this is a common behavior remains still unclear.

Thus, although the general characteristics seem well established, some questions remain still open. In particular, a comparative study of the adsorption of TCNQ on different metal surfaces is still lacking. An important theoretical study on the adsorption of F4-TCNQ on the coinage metals Cu(111), Ag(111), and Au(111)[40] was somewhat hampered by the fact that no dispersion forces were taken into account in the calculations, which makes the adsorption geometry to be slightly different from the results reported here. Also, while adsorption on the Cu(111) surface has been thoroughly studied theoretically,[46,51] reports on the Au(111) and Ag(111) surfaces are more scarce,[43,48] and a direct comparison is difficult by the use of different calculation methods. In addition, the comparison of the different systems is further complicated by the fact that the molecular assembly is different in every system, and even for the same system, several phases can coexist on the surface.[37,44,46,48,51,55,56]

DOI: 10.1021/acsomega.9b02154
ACS Omega 2019, 4, 16906−16915

Here, we show a comparative computational study based on the density functional theory (DFT) of the adsorption of TCNQ and F4-TCNQ on the (111) surfaces of the coinage metals, namely, copper, silver, and gold. To make a direct comparison possible, we try to separate the molecule−substrate interaction from the molecule−molecule interaction, and thus, in this work, we focus only on the adsorption of isolated molecules, not taking into account the different phases reported as the coverage increases. In addition, the presence of substrate adatoms is also neglected. Since the possible appearance of adatoms is strongly temperature-dependent,[59,60] we do not expect them to be relevant at low enough temperatures.

RESULTS AND DISCUSSION

Table 1 and Figure 2 show the bond lengths calculated for the neutral gas-phase TCNQ and F4-TCNQ molecules and their anions. The results compare well with the experimental data, the average difference between experimental measurements and calculated bond lengths being 0.02 Å.[61−63] As already reported,[64] the introduction of a negative charge leads to the partial aromatization of the central C ring and the lengthening of the B3 bond, which acquires a marked single-bond character. The extra negative charge is mostly accommodated over the two dicyanomethylene groups. Actually, a Mulliken population analysis reveals that each N atom in the anion and dianion forms of TCNQ carries charges of 0.27 and 0.39 electrons, respectively. The electron affinity, calculated as EA = $E(N) - E(N + 1)$, where $E(N_i)$ is the ground state of the molecule with N_i electrons,[43] is 3.45 eV, which agrees with previous experimental measurements[23] and calculations.[65,66]

The minimum energy optimized structures upon adsorption of TCNQ on Cu(111), Ag(111), and Au(111) are shown in Figure 3. For Au and Ag, the long molecular axis is parallel to

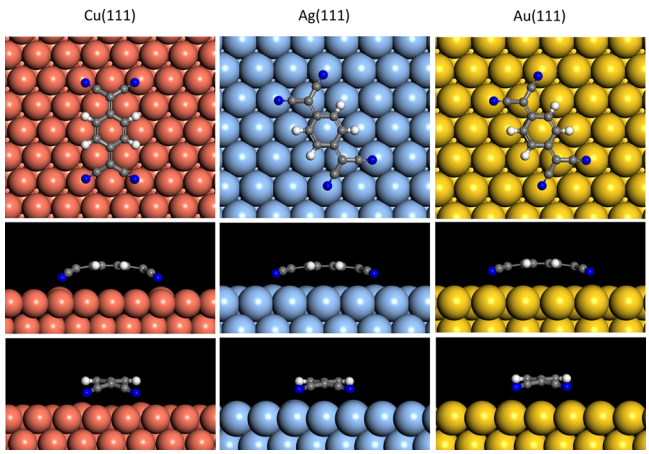

Figure 3. Top and side views of the calculated minimum energy adsorption geometry of TCNQ on Cu(111), Ag(111), and Au(111).

the ⟨1 $\bar{1}$0⟩ direction (configuration 1), while for Cu it is parallel to the ⟨12$\bar{1}$⟩ direction (configuration 2). The difference in the adsorption geometry is due to the smaller lattice parameter of Cu: In the gas phase, the four nitrogen atoms of TCNQ form a rectangle of 8.34 Å × 4.43 Å. In the Ag(111) surface, the four silver atoms directly underneath the N form a rectangle (before adsorption) of 8.67 Å (+4.0%) × 5.00 Å (+12.9%). For Au(111), the numbers are 8.80 Å (+5.51%) × 5.08 Å (+14.67%). For Cu(111), the corresponding distances in this same adsorption geometry would be 7.56 Å (−9.4%) × 4.37 Å (−1.4%). However, for the minimum energy configuration, the rectangle formed by the copper atoms underneath the N atoms has dimensions of 8.73 Å (+4.7%) × 5.04 Å (+13.8%). Although the van der Waals contribution always favors configuration 1, this small difference is enough to change the minimum energy configuration and seems to be related not only to the lattice misfit but also to the sign of this misfit since the more electronegative part of the TCNQ molecule, and hence the more reactive part, is directed outward the nitrogen atoms (Figure 1). The difference in adsorption energy between the two configurations, however, is rather small (≈0.12 eV), in accordance with previous results.[46]

Figure 3 also shows that, in all cases, the molecule is clearly bent, with the carbon ring parallel to the metal surface and the cyano groups pointing toward the metal atoms underneath. Figure 4 shows a summary of the main distances

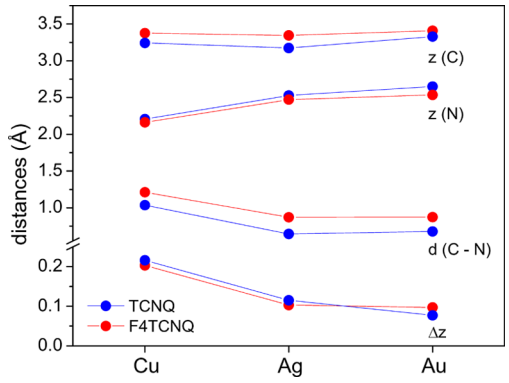

Figure 4. Geometric distances characterizing the adsorption of TCNQ and F4-TCNQ on the Cu, Ag, and Au metal surfaces: z(C) = height of the C atoms in the central ring above the top metal surface; z(N) = height of the N atoms above the top metal surface; d(C−N) = height difference between the N atoms and the C in the central ring; Δz = height of the topmost surface metal atom over the average surface plane.

characterizing the adsorption of TCNQ on the different surfaces: z(C), the height of the central C ring above the average surface plane; z(N), the height of the four nitrogen atoms above the average surface plane; d(C−N), the vertical distance between the central C ring and the N atoms; and Δz, the maximum height of the metal atoms above the average surface plane (not to be confused with the total rumpling of the metal surface, the maximum height difference between the atoms of the top metal surface, which is 0.35 Å for Cu, 0.24 Å for Ag, and 0.21 Å in the case of Au. The total rumpling of the second metal layer is much smaller: 0.082, 0.066, and 0.068, respectively). The figure shows that the height of the molecular core above the metal surface is approximately the same (3.2−3.4 Å) in all cases, although TCNQ is slightly closer to the surface than F4-TCNQ; also, on the three surfaces the N atoms are closer to the metal surface than the C ring, although the bending is markedly stronger for Cu, which shows the largest difference between the heights of the N atoms and the C ring (1.036 Å) and the lowest distance between the N atoms and the topmost surface layer (2.21 Å). At the same time, the interaction between the molecule and the surface pulls out some metal atoms of the average surface plane, especially those directly underneath the N atoms. The combinations of the molecular bending and substrate distortion lead to a minimum

DOI: 10.1021/acsomega.9b02154
ACS Omega 2019, 4, 16906−16915

nitrogen−metal distance of 2.05 Å in the case of Cu, 2.46 Å for Ag, and 2.67 Å for Au. Note that, in the case of Cu, this minimum Cu−N distance is very close to the sum of the covalent radii of N and Cu,[67] effectively suggesting the formation of a true chemical bond. The results also indicate that the adsorption geometry of F4-TCNQ on the three surfaces is very similar to TCNQ's (as previously reported),[40] although the amount of bending is slightly larger (see Figure 4). Experimental results have been obtained for F4-TCNQ on Cu(111), giving a height of 3.6 Å for the F atoms and 2.1 Å for the C atoms.[38] Our results in these case give 3.4 and 2.2 Å, respectively, in good agreement with the experiments.

Note that, in the absence of the metal surface, the bending of the molecule is energetically unfavorable: the energy of an isolated TCNQ molecule with the bent configuration that it adopts on the Cu (Ag, Au) surface is higher by 0.66 eV (0.35, 0.20 eV) than the energy of an isolated planar gas-phase molecule; for F4-TCNQ, the numbers are 0.64 (Cu), 0.37 (Ag), and 0.27 (Au) eV. Of course, this costly increase in energy is more than compensated by the interaction with the surface. Also, due to the concentration of the negative charge on the dicyano groups, even for an isolated neutral molecule in the gas phase, this structural distortion would create a dipole moment of 3.2 Db in the Cu case and of ∼2.1 Db for Ag and Au (3.3, 2.25, and 2.28 Db for F4-TCNQ).

As mentioned above, the in-plane molecular structure is also modified. As shown in Table 1 and Figure 2 for TCNQ, there is a partial aromatization of the C ring and a clear lengthening of the B3 bond. In the case of the gold surface, the bond lengths are close to those in the anion state of the isolated TCNQ molecule, while for Ag and Cu they are very similar to the molecule's in the dianion form. As a whole, if the bending of the molecule implies a strong interaction with the metal surface, the in-plane distortion seems to indicate a partial charging of the molecule, both effects decreasing in the order Cu, Ag, and Au.

The adsorption energies for TCNQ (blue symbols) and F4-TCNQ (red symbols) on the three metal surfaces calculated as $E_{ad} = (E_{mol} + E_{metal}) - E_{mol/metal}$, where $E_{mol/metal}$ is the energy of the complete system and E_{mol} and E_{metal}, are the energies of the molecule and the metal surfaces in their isolated, relaxed configurations, respectively, are displayed in Figure 5 (note that the results of both calculation methods (full symbols for DMol3; empty symbols for CASTEP) agree within ∼0.1 eV). For TCNQ, the binding energies are 3.57, 2.80, and 1.88 eV for Cu, Ag, and Au, respectively, which agree fairly well with values previously reported for TCNQ on Ag(111) (2.51 eV)[48] and Cu(111) (3.30−3.72 eV).[46,51] For F4-TCNQ, the binding energies are systematically larger than for TCNQ: 4.07 (Cu), 3.21 (Ag), and 2.21 eV (Au). Within the TS scheme, van der Waals interactions (triangular symbols) are almost the same for both molecules. Thus, the difference between TCNQ and F4-TCNQ is preserved when no dispersion interactions are taken into account (square symbols) and is due to the more electronegative character of the fluorine atoms. Also, van der Waals interactions are very similar on the Ag(111) and Au(111) surfaces, while on Cu(111) they add an additional contribution of ∼0.4 eV to the total binding energy.

Figure 6 shows the projected density of states (PDOS), calculated using the DMol3 software, for both TCNQ (left panel) and F4-TCNQ (right panel) adsorbed on the three metal surfaces. Very similar results (not shown) are obtained using CASTEP. Unrestricted spin calculations were also made,

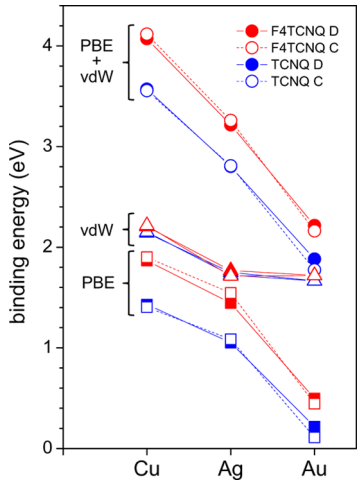

Figure 5. Calculated binding energies upon adsorption of TCNQ (blue circles) and F4-TCNQ (red circles) on Cu(111), Ag(111), and Au(111). The letters in the graph labels refer to the software used in the calculations (D = DMol3 (full symbols); C = CASTEP (empty symbols)). The square symbols are the corresponding binding energies when van der Waals interactions are not taken into account, while triangular symbols indicate only the van der Waals contribution.

but no spin polarization was found in any case. Although broader and shifted down in energy, by comparing with the densities of states calculated for the isolated gas-phase molecules (top panels in Figure 6), the frontier-related molecular orbitals after adsorption are easily recognized, especially for Ag and Au. (As an example, Figure 7 shows two different isosurfaces for those electronic levels assigned to the HOMO- and LUMO-related orbitals in the TCNQ/Ag(111) system). Note, however, that the hybridization of the molecular orbitals with the metal states is much larger for Cu where the HOMO-related orbital is barely distinguished. In the case of Ag and Cu, the LUMO-related orbital falls well below the Fermi level, while for Au it seems to be only partially occupied.

The rearrangement of the electron density at the molecule/metal interface can be visualized by looking at the density difference graphs displayed in Figure 8. These graphs are obtained by substracting the charge densities of the isolated systems from the charge density of the combined system

$$\Delta\rho = \rho_{TCNQ/M(111)} - \rho_{TCNQ} - \rho_{M(111)} \quad (1)$$

where ρ_{TCNQ} and $\rho_{M(111)}$ (M stands for the different metals) are the charge densities of the individual systems calculated with the geometry they adopt in the combined system $\rho_{TCNQ/M(111)}$. The graphs in Figure 8 show the top and side views of three such density difference isosurfaces, corresponding to an electron density difference of 0.01 electrons/Å^3 in which the red areas show places where the electron density has been enriched while the blue areas show where the density has been depleted. By comparing with the shape of the orbitals for the gas-phase isolated molecule (Figure 1), it can be concluded that the LUMO-related orbital is almost completely occupied after adsorption, approximately by the same amount, in Cu and Ag, but it is only partially filled on Au. The electrons come mainly from a region slightly above the surface plane close to the metal atoms underneath the N atoms. There is also electron depletion in the bonds that lengthen upon adsorption (B1, B3, and B5, see Figure 2). The graphs clearly show that

DOI: 10.1021/acsomega.9b02154
ACS Omega 2019, 4, 16906−16915

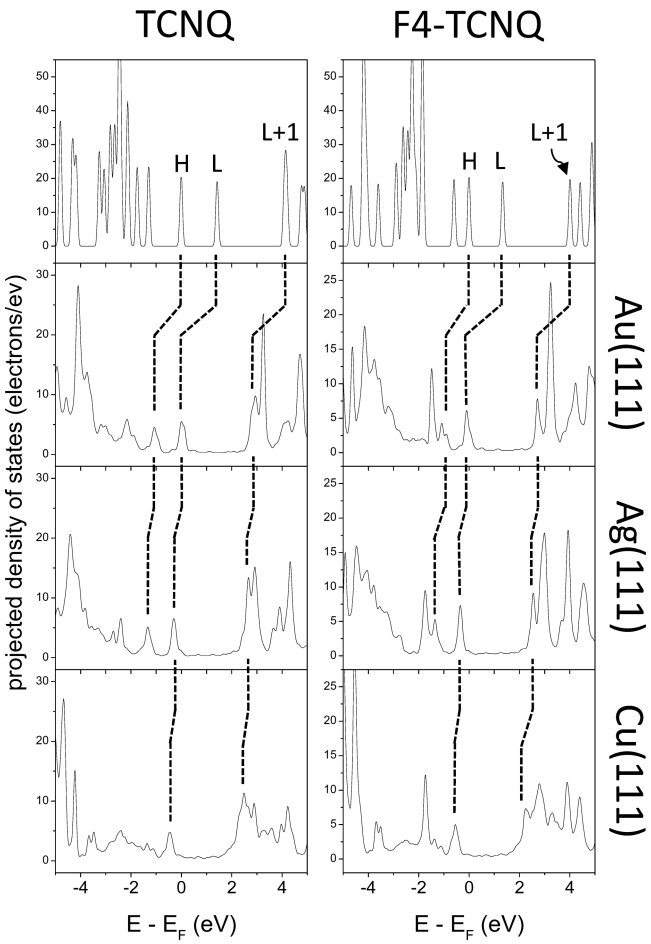

Figure 6. Projected density of states of TCNQ (left) and F4-TCNQ (right) when adsorbed on Cu(111), Ag(111), and Au(111). The energy scale is referred to the Fermi level. In both cases, the top panels show the density of states for the neutral isolated molecule. In these graphs, the energy scale is referred to the position of the HOMO orbital. The dashed lines indicate the proposed correspondence between the molecular orbitals and the orbitals after adsorption.

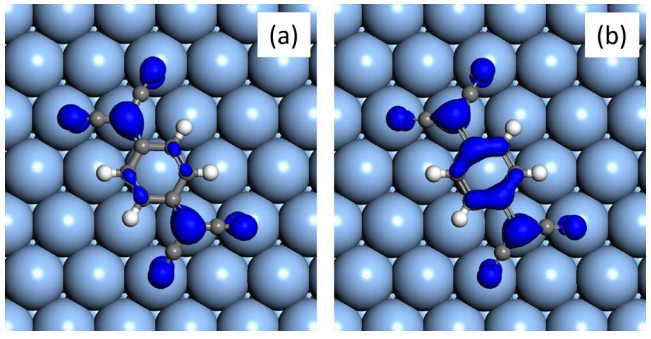

Figure 7. Two isosurfaces, corresponding to an electron density of 0.004 electrons/Å^3, for those electron levels with an energy between (a) −1.51 and −1.03 eV and (b) −0.47 and 0.04 eV in the case of TCNQ/Ag(111). The resemblance with the HOMO and LUMO orbitals, respectively, of the TCNQ molecule (see Figure 1) seems clear.

there is some amount of electron backdonation, much larger for the copper surface than for silver and gold. This can be also visualized by making cuts of the electron density difference along planes parallel to the metal surface. Figure 9 shows one

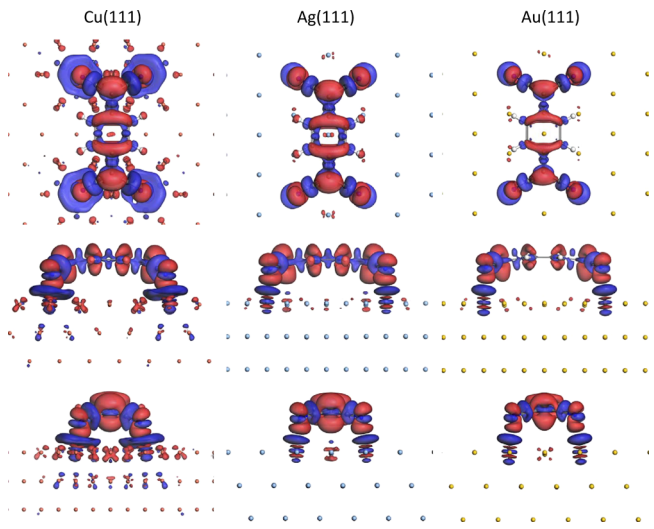

Figure 8. Charge density difference graphs (top and side views) for TCNQ adsorption on Cu(111), Ag(111), and Au(111). The isosurfaces drawn correspond to an electron density difference of 0.01 electrons/Å^3. The red areas show where the electron density has been enriched, while the blue areas show where the density has been depleted.

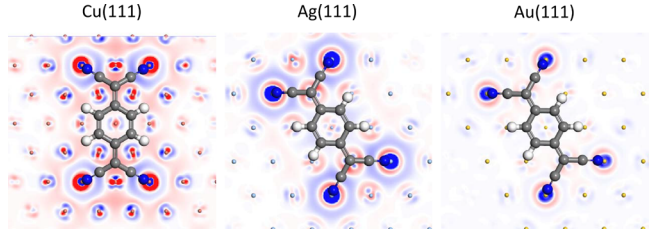

Figure 9. Horizontal cuts of the electron density difference across the topmost metal plane. Regions of electron depletion are depicted in blue, while areas of electron enrichment are drawn in red. The color scale goes from −0.01 to 0.01 electrons/Å^3.

of these cuts across the topmost metal plane. There are regions on the metal surface, especially in the case of copper, that have gained electrons after the molecular adsorption. These results agree with previous calculations that show that, in the F4-TCNQ case, backdonation comes mainly from the orbitals HOMO-9 to HOMO-12, which are mainly localized around the cyano groups (explaining the lengthening of the B5 bond).[40]

As a consequence of electron backdonation, the net amount of charge transfer cannot be interpreted directly as a sign of the strength of the molecule−metal interaction and is not directly correlated to the binding energy. The amounts of charge transfer, calculated using both the DMol3 and CASTEP software, are shown in Figure 10. For the two calculation methods, we have followed the Hirshfeld[68] partition system of the electron density. In addition, in the case of DMol3, we have also used the Mulliken analysis.[69] Both the Mulliken and Hirshfeld methods calculate a very similar charge transfer for Cu and Ag, while in the case of Au the Hirshfeld charge is noticeably larger (0.3−0.4 e) than the Mulliken charge. However, it is well known that the different partition schemes can give very different partial charges,[70] and so, only the relative trends between the three metal surfaces are really meaningful. From the results, we can conclude that, in three cases, the charge transferred to the F4-TCNQ molecule is

DOI: 10.1021/acsomega.9b02154
ACS Omega 2019, 4, 16906−16915

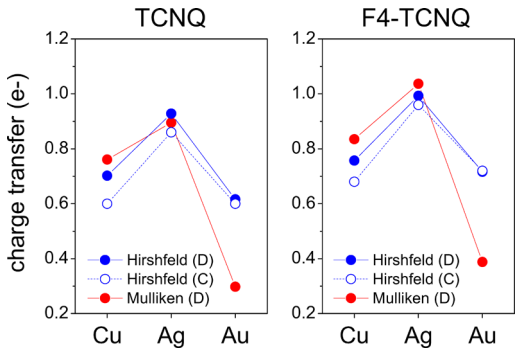

Figure 10. Calculated charge transfer upon adsorption of TCNQ (left) and F4-TCNQ (right) on Cu(111), Ag(111), and Au(111). The letters in the graph labels refer to the software used in the calculations (D = DMol3; C = CASTEP).

somewhat larger than the charge transferred to TCNQ. Also, the charge transfer seems to be largest in the case of Ag and slightly less for Cu and Au (which agrees with previous results published for F4-TCNQ).[40] The similarity between Cu and Au, however, can be somewhat misleading. The charge transfer in Au is due to the LUMO orbital being only partially occupied. In Cu, however, the LUMO is completely filled, but there is a considerable amount of electron backdonation to the metal. Ag, on the other hand, is an intermediate case: the LUMO is also completely filled, but the amount of backdonation is smaller than that in Cu.

The calculated work functions after adsorption are shown in Figure 11. The change in work function has two different

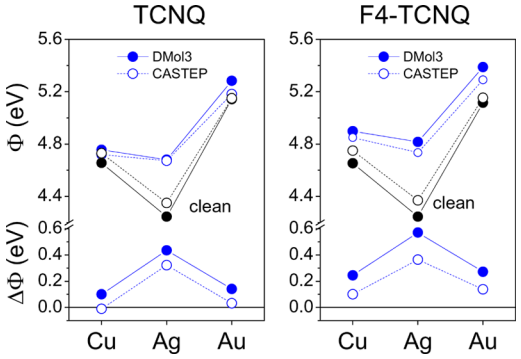

Figure 11. Calculated work functions upon adsorption of TCNQ (left) and F4-TCNQ (right) on Cu(111), Ag(111), and Au(111).

origins. The first one, the so-called molecular contribution, is due to the possible existence of molecular dipolar moments. As mentioned above, although TCNQ and F4-TCNQ are planar molecules when isolated, with no dipolar moment, due to the concentration of the negative charge on the dicyano groups, the structural distortion suffered upon adsorption creates a dipole moment even in the absence of charge transfer. This dipole points away from the surface and thus tends to decrease the work function of the substrate. The second origin is the rearrangement of the electron density at the interface: charge transfer from the substrate to the molecule tends to increase the work function. The contribution of both effects makes the change in the work functions of Cu and Ag to be very small but larger for Ag due to the larger amount of charge transfer.

The results presented here agree qualitatively with most of the available theoretical and experimental data, the only significant discrepancy being the TCNQ/Au(111) system, where the experimental results point to a physisorbed state with null charge transfer[39] and a work function decrease.[44,55] This discrepancy is related to the so-called energy gap problem.[71,72] Although the combination GGA-PBE is used in many studies of molecular adsorption on metal surfaces, it is well known that the PBE functional underestimates the band gaps of semiconductors and insulators and, in particular, the HOMO−LUMO band gaps of organic molecules. However, it has been shown that, when dealing with metal−organic interfaces (especially in the case of copper and silver), image potential effects and polarization effects can compensate the self-interaction corrections origin of this energy gap problem.[73,74] The TCNQ/Au(111) system must be a limiting case, since already for F4-TCNQ/Au(111) the experimental results indicate a certain amount of charge transfer[31] and a work function increase,[55] in accordance with our calculations. This is demonstrated in Figure 12, which shows the density of states (DOS) of the TCNQ and F4-TCNQ molecules together with the DOS of the clean metal surfaces. When using the PBE functional, the LUMO orbitals of both molecules fall below the Fermi level of the three metal surfaces but only by ∼0.2 eV for TCNQ on Au(111). For the remaining systems, this shifting does not modify significantly our conclusions.

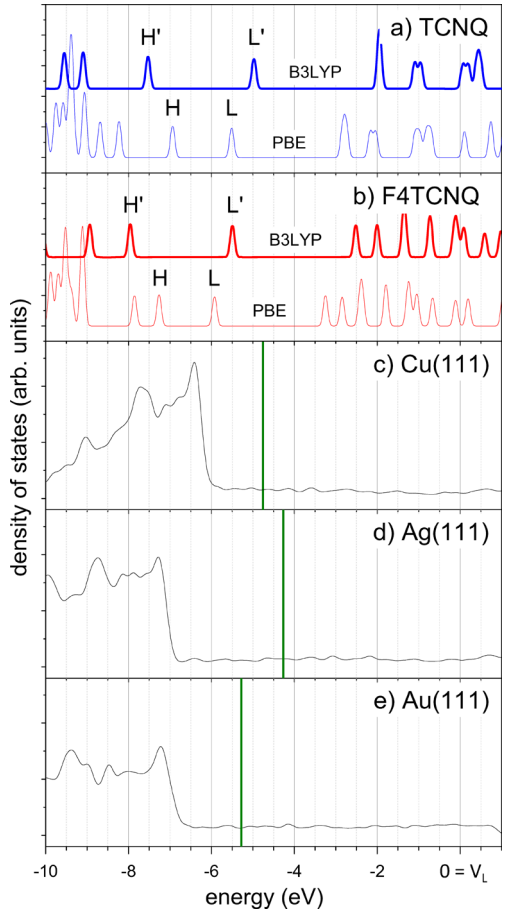

Figure 12. Calculated densities of states of the (a) TCNQ and (b) F4-TCNQ free gas-phase molecules using two different functionals (PBE, B3LYP) and of (c−e) the clean metal surfaces (only PBE). The common origin of energies is the vacuum level V_L. The green vertical lines indicate the Fermi levels of the three metals. The dashed vertical lines are guides to the eye.

DOI: 10.1021/acsomega.9b02154
ACS Omega 2019, 4, 16906−16915

Among other alternatives, the use of hybrid orbitals, which combine the generalized gradient functional with the exact (Hartree−Fock) exchange, helps to solve this energy gap problem.[75] For example, if the molecular DOS are calculated using the hybrid B3LYP functional, the energy gap widens by ∼1.1 eV and the LUMO orbital shifts ∼0.5 upward in energy, falling above the gold Fermi energy, in agreement with the experimental results for TCNQ/Au(111). Unfortunately, the B3LYP functional fails for bulk metals,[76] and other options are computationally much more demanding. Thus, the results presented here, especially those regarding charge transfer between the metals and the molecules, are to be taken only as guides to understand the general trends.

CONCLUSIONS

In summary, we have carried out a computational dispersion-corrected DFT study of the adsorption of isolated TCNQ and F4-TCNQ molecules on the Cu(111), Ag(111), and (unreconstructed) Au(111) surfaces. It seems clear from the results that the molecule−substrate interaction decreases in the order Cu > Ag > Au. Although this sequence seems fairly intuitive, it is convenient to remind that the interaction is strongly molecular-dependent. For example, in the case of TTF (tetrathiafulvalene)[77] or DIP (diindenoperylene),[78] the adsorption energies follow Cu > Au > Ag; meanwhile, for viologen[77] and triarylamines,[79] the order is Au > Cu > Ag. In our case, being TCNQ and F4-TCNQ relatively small molecules with a strong acceptor character, the weaker interaction with the gold surface seems to be related to the higher work function, while the difference between Ag and Cu lies on the amount of backdonation.

COMPUTATIONAL DETAILS

DFT calculations were carried out using the DMol3 package integrated in the Material Studio program of Accelrys Inc.[80,81] The electron exchange and correlation energies were treated with the generalized gradient approximation (GGA) of Perdew, Burke, and Ernzerhof.[82] The valence electron functions were expanded to a set of numerical atomic orbitals by a double-numerical basis with polarization functions (DNP), (a polarization d function on all the non-hydrogen atoms and a polarization p function on all the hydrogen atoms). The cutoff radius was set to Rc = 5.3 Å. DFT semicore pseudopotentials (DSPP),[83] which include some degree of relativistic effects, were used for Cu, Ag, and Au. The Tkatchenko and Scheffler (TS) scheme[84] for dispersion correction was also included. The convergence criteria were as follows: SCF tolerance, 2×10^{-5} eV; maximum displacement, 2×10^{-3} Å; maximum force, 2.7×10^{-2} eV/Å; and total energy, 2×10^{-5} eV. Under these conditions, the lattice parameters of bulk Cu, Ag, and Au are 3.564, 4.113, and 4.146 Å, in close agreement (within −1.41, 0.68, and 1.66%, respectively) with the experimental values (3.615, 4.085, and 4.078 Å).

The metal surfaces were simulated by a repeated six layers slab where the four bottom layers were kept frozen, with a lateral 6 × 7 supercell and a unit cell length in a perpendicular direction of 50 Å, in order to avoid the interaction between adjacent structures. Thus, due to the high computational cost, we are neglecting the long-range order imposed by the herringbone reconstruction of the gold surface.[85] Nevertheless, it has been shown that many organic molecules, including strong acceptors like (the closely related) TCNE[86] or PCBM,[87] tend to nucleate on the fcc areas of the reconstruction, which is what we are simulating here. The Brillouin zone was sampled by 8 × 7 × 3 Monkhorst−Pack mesh.[88] The values of the work functions for the clean metal surfaces, calculated using the Neugebauer−Scheffler dipole correction,[89] are 4.76 eV for Cu(111), 4.27 eV for Ag(111), and 5.21 eV for Au(111), which agree fairly well with previous results.[90,91]

Once the adsorption geometries were fully relaxed, the electronic structure calculations were repeated using the CASTEP package also included in the Materials Studio program.[92] In this case, ultrasoft pseudopotentials with the PBE funcional and the TS scheme for dispersion correction were used.[93] The plane wave basis set was expanded to a 360 eV kinetic energy cutoff, and a 2 × 2 × 1 Monkhorst−Pack grid was used.

AUTHOR INFORMATION

Corresponding Author

*E-mail: josemaria.gallego@csic.es.

ORCID

José M. Gallego: 0000-0003-1716-0126

Notes

The authors declare no competing financial interest.

ACKNOWLEDGMENTS

This work has been financed by the Spanish Ministerio de EconomIndustria y Competitividad (Project FIS2016-78591-C3-1-R) and the Comunidad de Madrid (Project S2013/MT-2850).

REFERENCES

(1) Embracing the organics world. *Nat. Mater.* **2013**, *12*, 591, DOI: 10.1038/nmat3707.

(2) Nisato, G.; Lupo, D.; Ganz, S. *Organic and Printed Electronics: Fundamentals and Applications*; Pan Stanford Publishing: New York, 2016.

(3) Ling, H.; Liu, S.; Zheng, Z.; Yan, F. Organic Flexible Electronics. *Small Methods* **2018**, *2*, 1800070.

(4) Zhang, J.; Xu, W.; Sheng, P.; Zhao, G.; Zhu, D. Organic Donor-Acceptor Complexes as Novel Organic Semiconductors. *Acc. Chem. Res.* **2017**, *50*, 1654−1662.

(5) Inganäs, O. Organic Photovoltaics over Three Decades. *Adv. Mater.* **2018**, *30*, 1800388.

(6) Ishii, H.; Sugiyama, K.; Ito, E.; Seki, K. Energy level alignment and interfacial electronic structures at organic/metal and organic/organic interfaces. *Adv. Mater.* **1999**, *11*, 605−625.

(7) Koch, N. Organic electronic devices and their functional interfaces. *ChemPhysChem* **2007**, *8*, 1438−1455.

(8) Braun, S.; Salaneck, W. R.; Fahlman, M. Energy-Level Alignment at Organic/Metal and Organic/Organic Interfaces. *Adv. Mater.* **2009**, *21*, 1450−1472.

(9) Di, C.-a.; Liu, Y.; Yu, G.; Zhu, D. Interface Engineering: An Effective Approach toward High-Performance Organic Field-Effect Transistors. *Acc. Chem. Res.* **2009**, *42*, 1573−1583.

(10) Hwang, J.; Wan, A.; Kahn, A. Energetics of metal-organic interfaces: New experiments and assessment of the field. *Mater. Sci. Eng., R* **2009**, *64*, 1−31.

(11) Gao, Y. Surface analytical studies of interfaces in organic semiconductor devices. *Mater. Sci. Eng., R* **2010**, *68*, 39−87.

(12) Amsalem, P.; Heimel, G.; Oehzelt, M.; Koch, N. The interface electronic properties of organic photovoltaic cells. *J. Electron Spectrosc. Relat. Phenom.* **2015**, *204*, 177−185.

DOI: 10.1021/acsomega.9b02154
ACS Omega 2019, 4, 16906−16915

(13) Goiri, E.; Borghetti, P.; El-Sayed, A.; Ortega, J. E.; de Oteyza, D. G. Multi-Component Organic Layers on Metal Substrates. *Adv. Mater.* **2016**, *28*, 1340−1368.
(14) Hu, Z.; Zhong, Z.; Chen, Y.; Sun, C.; Huang, F.; Peng, J.; Wang, J.; Cao, Y. Energy-Level Alignment at the Organic/Electrode Interface in Organic Optoelectronic Devices. *Adv. Funct. Mater.* **2016**, *26*, 129−136.
(15) Otero, R.; Vázquez de Parga, A. L.; Gallego, J. M. Electronic, structural and chemical effects of charge-transfer at organic/inorganic interfaces. *Surf. Sci. Rep.* **2017**, *72*, 105−145.
(16) Tseng, T.-C.; Urban, C.; Wang, Y.; Otero, R.; Tait, S. L.; Alcamí, M.; Écija, D.; Trelka, M.; Gallego, J. M.; Lin, N.; et al. Charge-transfer-induced structural rearrangements at both sides of organic/metal interfaces. *Nat. Chem.* **2010**, *2*, 374−379.
(17) Acker, D. S.; Hertler, W. R. Substituted Quinodimethans. I. Preparation and Chemistry of 7,7,8,8-Tetracyanoquinodimethan. *J. Am. Chem. Soc.* **1962**, *84*, 3370−3374.
(18) Kepler, R. G.; Bierstedt, P. E.; Merrifield, R. E. Electronic Conduction and Exchange Interaction in a New Class of Conductive Organic Solids. *Phys. Rev. Lett.* **1960**, *5*, 503−504.
(19) Epstein, A. J.; Etemad, S.; Garito, A. F.; Heeger, A. J. Metal-insulator transition in an organic solid: Experimental realization of the one-dimensional Hubbard model. *Solid State Commun.* **1971**, *9*, 1803−1808.
(20) Ferraris, J.; Cowan, D. O.; Walatka, V.; Perlstein, J. H. Electron transfer in a new highly conducting donor-acceptor complex. *J. Am. Chem. Soc.* **1973**, *95*, 948−949.
(21) Farragher, A. L.; Page, F. M. Experimental determination of electron affinities. Part 11.-Electron capture by some cyanocarbons and related compounds. *Trans. Faraday Soc.* **1967**, *63*, 2369−2378.
(22) Klots, C. E.; Compton, R. N.; Raaen, V. F. Electronic and ionic properties of molecular TTF and TCNQ. *J. Chem. Phys.* **1974**, *60*, 1177−1178.
(23) Zhu, G.-Z.; Wang, L.-S. Communication: Vibrationally resolved photoelectron spectroscopy of the tetracyanoquinodimethane (TCNQ) anion and accurate determination of the electron affinity of TCNQ. *J. Chem. Phys.* **2015**, *143*, 221102.
(24) Starodub, V. A.; Starodub, T. N. Radical anion salts and charge transfer complexes based on tetracyanoquinodimethane and other strong π-electron acceptors. *Russ. Chem. Rev.* **2014**, *83*, 391.
(25) Tanner, D. B.; Jacobsen, C. S.; Garito, A. F.; Heeger, A. J. Infrared Conductivity of Tetrathiofulvalene Tetracyanoquinodimethane (TTF - TCNQ) Films. *Phys. Rev. Lett.* **1974**, *32*, 1301−1305.
(26) Miller, J. S.; Epstein, A. J. Organometallic magnets. *Coord. Chem. Rev.* **2000**, *206-207*, 651−660.
(27) Gibson, T. D.; Hulbert, J. N.; Parker, S. M.; Woodward, J. R.; Higgins, I. J. Extended shelf life of enzyme-based biosensors using a novel stabilization system. *Biosens. Bioelectron.* **1992**, *7*, 701−708.
(28) Gao, W.; Kahn, A. Controlled p-doping of zinc phthalocyanine by coevaporation with tetrafluorotetracyanoquinodimethane: A direct and inverse photoemission study. *Appl. Phys. Lett.* **2001**, *79*, 4040−4042.
(29) Blochwitz, J.; Pfeiffer, M.; Fritz, T.; Leo, K. Low voltage organic light emitting diodes featuring doped phthalocyanine as hole transport material. *Appl. Phys. Lett.* **1998**, *73*, 729−731.
(30) Gao, W.; Kahn, A. Controlled p doping of the hole-transport molecular material N,N'-diphenyl-N,N'-bis(1-naphthyl)-1,1′-biphenyl-4,4′-diamine with tetrafluorotetracyanoquinodimethane. *J. Appl. Phys.* **2003**, *94*, 359−366.
(31) Koch, N.; Duhm, S.; Rabe, J. P.; Vollmer, A.; Johnson, R. L. Optimized Hole Injection with Strong Electron Acceptors at Organic-Metal Interfaces. *Phys. Rev. Lett.* **2005**, *95*, 237601.
(32) Rana, O.; Srivastava, R.; Chauhan, G.; Zulfequar, M.; Husain, M.; Srivastava, P. C.; Kamalasanan, M. N. Modification of metal-organic interface using F4-TCNQ for enhanced hole injection properties in optoelectronic devices. *Phys. Status Solidi A* **2012**, *209*, 2539−2545.
(33) Grover, R.; Srivastava, R.; Kamalasanan, M. N.; Mehta, D. S. Novel organic electron injection layer for efficient and stable organic light emitting diodes. *J. Lumin.* **2014**, *146*, 53−56.
(34) Zhang, J.; Xin, L.; Gao, J.; Liu, Y.; Rui, H.; Lin, X.; Hua, Y.; Wu, X.; Yin, S. Improving the performance of organic light-emitting devices by incorporating non-doped TCNQ as electron buffer layer. *J. Mater. Sci.: Mater. Electron.* **2017**, *28*, 12761−12767.
(35) Erley, W.; Ibach, H. Vibrational-Spectra of Tetracyanoquinodimethane (TCNQ) Adsorbed on the Cu(111) Surface. *Surf. Sci.* **1986**, *178*, 565−577.
(36) Giergiel, J.; Wells, S.; Land, T. A.; Hemminger, J. C. Growth and chemistry of TCNQ films on nickel (111). *Surf. Sci.* **1991**, *255*, 31−40.
(37) Kamna, M. M.; Graham, T. M.; Love, J. C.; Weiss, P. S. Strong electronic perturbation of the Cu{111} surface by 7,7′,8,8′-tetracyanoquinonedimethane. *Surf. Sci.* **1998**, *419*, 12−23.
(38) Romaner, L.; Heimel, G.; Brédas, J.-L.; Gerlach, A.; Schreiber, F.; Johnson, R. L.; Zegenhagen, J.; Duhm, S.; Koch, N.; Zojer, E. Impact of bidirectional charge transfer and molecular distortions on the electronic structure of a metal-organic interface. *Phys. Rev. Lett.* **2007**, *99*, 256801−256801.
(39) Torrente, I. F.; Franke, K. J.; Pascual, J. I. Structure and electronic configuration of tetracyanoquinodimethane layers on a Au(111) surface. *Int. J. Mass Spectrom.* **2008**, *277*, 269−73.
(40) Rangger, G. M.; Hofmann, O. T.; Romaner, L.; Heimel, G.; Bröker, B.; Blum, R.-P.; Johnson, R. L.; Koch, N.; Zojer, E. F4TCNQ on Cu, Ag, and Au as prototypical example for a strong organic acceptor on coinage metals. *Phys. Rev. B* **2009**, *79*, 165306.
(41) Katayama, T.; Mukai, K.; Yoshimoto, S.; Yoshinobu, J. Thermally Activated Transformation from a Charge-Transfer State to a Rehybridized State of Tetrafluoro-tetracyanoquinodimethane on Cu(100). *J. Phys. Chem. Lett.* **2010**, *1*, 2917−2921.
(42) Katayama, T.; Mukai, K.; Yoshimoto, S.; Yoshinobu, J. Reactive rearrangements of step atoms by adsorption and asymmetric electronic states of tetrafluoro-tetracyanoquinodimethane on Cu(100). *Phys. Rev. B* **2011**, *83*, 153403.
(43) Martínez, J. I.; Abad, E.; Flores, F.; Ortega, J. Simulating the organic-molecule/metal interface TCNQ/Au(111). *Phys. Status Solidi B* **2011**, *248*, 2044−2049.
(44) Wäckerlin, C.; Iacovita, C.; Chylarecka, D.; Fesser, P.; Jung, T. A.; Ballav, N. Assembly of 2D ionic layers by reaction of alkali halides with the organic electrophile 7,7,8,8-tetracyano-p-quinodimethane (TCNQ). *Chem. Commun.* **2011**, *47*, 9146−9148.
(45) Faraggi, M. N.; Jiang, N.; Gonzalez-Lakunza, N.; Langner, A.; Stepanow, S.; Kern, K.; Arnau, A. Bonding and Charge Transfer in Metal-Organic Coordination Networks on Au(111) with Strong Acceptor Molecules. *J. Phys. Chem. C* **2012**, *116*, 24558−24565.
(46) Sara, B.; Barja, S.; Borca, B.; Garnica, M.; Díaz, C.; Rodriguez-García, J. M.; Alcamí, M.; Vázques de Parga, A. L.; Martin, F.; Miranda, R. Ordered arrays of metalorganic magnets at surfaces. *J. Phys.: Condens. Matter* **2013**, *25*, 484007.
(47) Burema, S. R.; Bocquet, M.-L. A sum rule for inelastic electron tunneling spectroscopy: an ab initio study of a donor (TTF) and acceptors (TCNE, TCNQ and DCNQI) parallelly oriented on Cu(100). *Phys. Chem. Chem. Phys.* **2013**, *15*, 16111−16119.
(48) Park, C.; Rojas, G. A.; Jeon, S.; Kelly, S. J.; Smith, S. C.; Sumpter, B. G.; Yoon, M.; Maksymovych, P. Weak competing interactions control assembly of strongly bonded TCNQ ionic acceptor molecules on silver surfaces. *Phys. Rev. B* **2014**, *90*, 125432.
(49) Sun, Z.; Zhan, Y.; Shi, S.; Fahlman, M. Energy level alignment and interactive spin polarization at organic/ferromagnetic metal interfaces for organic spintronics. *Org. Electron.* **2014**, *15*, 1951−1957.
(50) Feyer, V.; Graus, M.; Nigge, P.; Zamborlini, G.; Acres, R. G.; Schöll, A.; Reinert, F.; Schneider, C. M. The geometric and electronic structure of TCNQ and TCNQ+Mn on Ag(001) and Cu(001) surfaces. *J. Electron Spectrosc. Relat. Phenom.* **2015**, *204*, 125−131.
(51) Stradi, D.; Borca, B.; Barja, S.; Garnica, M.; Diaz, C.; Rodríguez-García, J. M.; Alcami, M.; Vázquez de Parga, A. L.; Miranda, R.; Martin, F. Understanding the selfassembly of TCNQ on

DOI: 10.1021/acsomega.9b02154
ACS Omega 2019, 4, 16906−16915

Cu(111): a combined study based on scanning tunnelling microscopy experiments and density functional theory simulations. *RSC Adv.* **2016**, *6*, 15071−15079.
(52) Gerbert, D.; Tegeder, P. Molecular Ion Formation by Photoinduced Electron Transfer at the Tetracyanoquinodimethane/Au(111) Interface. *J. Phys. Chem. Lett.* **2017**, *8*, 4685−4690.
(53) Borghetti, P.; Sarasola, A.; Merino-Díez, N.; Vasseur, G.; Floreano, L.; Lobo-Checa, J.; Arnau, A.; de Oteyza, D. G.; Ortega, J. E. Symmetry, Shape, and Energy Variations in Frontier Molecular Orbitals at Organic-Metal Interfaces: The Case of F4TCNQ. *J. Phys. Chem. C* **2017**, *121*, 28412−28419.
(54) Gerbert, D.; Maaβ, F.; Tegeder, P. Extended Space Charge Region and Unoccupied Molecular Band Formation in Epitaxial Tetrafluorotetracyanoquinodimethane Films. *J. Phys. Chem. C* **2017**, *121*, 15696−15701.
(55) Yamane, H.; Kosugi, N. High Hole-Mobility Molecular Layer Made from Strong Electron Acceptor Molecules with Metal Adatoms. *J. Phys. Chem. Lett.* **2017**, *8*, 5366−5371.
(56) Blowey, P. J.; Velari, S.; Rochford, L. A.; Duncan, D. A.; Warr, D. A.; Lee, T.-L.; De Vita, A.; Costantini, G.; Woodruff, D. P. Re-evaluating how charge transfer modifies the conformation of adsorbed molecules. *Nanoscale* **2018**, *10*, 14984−14992.
(57) Rodríguez-Fernández, J. Donor and Acceptor Molecules on Metal Surfaces: Supramolecular: Self-Assembly, Metal-Organic Coordination Networks, and Charge-Transfer Complexe. Ph.D. Thesis, 2014.
(58) Della Pia, A.; Riello, M.; Stassen, D.; Jones, T. S.; Bonifazi, D.; De Vita, A.; Costantini, G. Two-dimensional core-shell donor-acceptor assemblies at metal-organic interfaces promoted by surface-mediated charge transfer. *Nanoscale* **2016**, *8*, 19004−19013.
(59) Morgenstern, K.; Rosenfeld, G.; Lægsgaard, E.; Besenbacher, F.; Comsa, G. Measurement of Energies Controlling Ripening and Annealing on Metal Surfaces. *Phys. Rev. Lett.* **1998**, *80*, 556−559.
(60) Rodríguez-Fernández, J.; Lauwaet, K.; Herranz, M. Á.; Martín, N.; Gallego, J. M.; Miranda, R.; Otero, R. Temperature-controlled metal/ligand stoichiometric ratio in Ag-TCNE coordination networks. *J. Chem. Phys.* **2015**, *142*, 101930.
(61) Long, R. E.; Sparks, R. A.; Trueblood, K. N. The crystal and molecular structure of 7,7,8,8-tetracyanoquinodimethane. *Acta Crystallogr.* **1965**, *18*, 932−939.
(62) Miller, J. S.; Zhang, J. H.; Reiff, W. M.; Dixon, D. A.; Preston, L. D.; Reis, A. H.; Gebert, E.; Extine, M.; Troup, J.; et al. Characterization of the charge-transfer reaction between decamethylferrocene and 7,7,8,8,-tetracyano-p-quinodimethane (1:1). The iron-57 Moessbauer spectra and structures of the paramagnetic dimeric and the metamagnetic one-dimensional salts and the molecular and electronic structures of $(TCNQ)^n$ (n = 0, −1, −2). *J. Phys. Chem.* **1987**, *91*, 4344−4360.
(63) Hoekstra, A.; Spoelder, T.; Vos, A. The crystal structure of rubidium−7,7,8,8-tetracyanoquinodimethane, Rb−TCNQ, at −160°C. *Acta Crystallogr., Sect. B: Struct. Crystallogr. Cryst. Chem.* **1972**, *28*, 14−25.
(64) Milián, B.; Pou-Amérigo, R.; Viruela, R.; Ortí, E. A theoretical study of neutral and reduced tetracyano-p-quinodimethane (TCNQ). *J. Mol. Struct.: THEOCHEM* **2004**, *709*, 97−102.
(65) Milián, B.; Pou-Amérigo, R.; Viruela, R.; Ortí, E. On the electron affinity of TCNQ. *Chem. Phys. Lett.* **2004**, *391*, 148−151.
(66) Nakashima, H.; Honda, Y.; Shida, T.; Nakatsuji, H. Electronic excitation spectra of doublet anion radicals of cyanobenzene and nitrobenzene derivatives: SAC-CI theoretical studies. *Mol. Phys.* **2015**, *113*, 1728−1739.
(67) Cordero, B.; Gómez, V.; Platero-Prats, A. E.; Revés, M.; Echeverría, J.; Cremades, E.; Barragán, F.; Alvarez, S. Covalent radii revisited. *Dalton Trans.* **2008**, 2832−2838.
(68) Hirshfeld, F. L. Bonded-atom fragments for describing molecular charge densities. *Theor. Chim. Acta* **1977**, *44*, 129−138.
(69) Mulliken, R. S. Electronic Population Analysis on LCAO-MO Molecular Wave Functions. I. *J. Chem. Phys.* **1955**, *23*, 1833−1840.
(70) Wiberg, K. B.; Rablen, P. R. Comparison of atomic charges derived via different procedures. *J. Comput. Chem.* **1993**, *14*, 1504−1518.
(71) Perdew, J. P. Density functional theory and the band gap problem. *Int. J. Quantum Chem.* **1985**, *28*, 497−523.
(72) Perdew, J. P.; Yang, W.; Burke, K.; Yang, Z.; Gross, E. K. U.; Scheffler, M.; Scuseria, G. E.; Henderson, T. M.; Zhang, I. Y.; Ruzsinszky, A.; et al. Understanding band gaps of solids in generalized KohnSham theory. *Proc. Natl. Acad. Sci. U. S. A.* **2017**, *114*, 2801−2806.
(73) Flores, F.; Ortega, J.; Vázquez, H. Modelling energy level alignment at organic interfaces and density functional theory. *Phys. Chem. Chem. Phys.* **2009**, *11*, 8658−8675.
(74) Hofmann, O. T.; Atalla, V.; Moll, N.; Rinke, P.; Scheffler, M. Interface dipoles of organic molecules on Ag(111) in hybrid density-functional theory. *New J. Phys.* **2013**, *15*, 123028.
(75) Becke, A. D. A new mixing of Hartree-Fock and local density-functional theories. *J. Chem. Phys.* **1993**, *98*, 1372−1377.
(76) Paier, J.; Marsman, M.; Kresse, G. Why does the B3LYP hybrid functional fail for metals? *J. Chem. Phys.* **2007**, *127*, No. 024103.
(77) Hofmann, O. T.; Rangger, G. M.; Zojer, E. Reducing the Metal Work Function beyond Pauli Pushback: A Computational Investigation of Tetrathiafulvalene and Viologen on Coinage Metal Surfaces. *J. Phys. Chem. C* **2008**, *112*, 20357−20365.
(78) Björk, J.; Stafström, S. Adsorption of Large Hydrocarbons on Coinage Metals: A van der Waals Density Functional Study. *ChemPhysChem* **2014**, *15*, 2851−2858.
(79) Müller, K.; Moreno-López, J. C.; Gottardi, S.; Meinhardt, U.; Yildirim, H.; Kara, A.; Kivala, M.; Stöhr, M. Cyano-Functionalized Triarylamines on Coinage Metal Surfaces: Interplay of Intermolecular and Molecule-Substrate Interactions. *Chem. − Eur. J.* **2016**, *22*, 581−589.
(80) Delley, B. An all-electron numerical method for solving the local density functional for polyatomic molecules. *J. Chem. Phys.* **1990**, *92*, 508.
(81) Delley, B. From molecules to solids with the $DMol^3$ approach. *J. Chem. Phys.* **2000**, *113*, 7756.
(82) Perdew, J. P.; Burke, K.; Ernzerhof, M. Generalized Gradient Approximation Made Simple. *Phys. Rev. Lett.* **1996**, *77*, 3865−3868.
(83) Delley, B. Hardness conserving semilocal pseudopotentials. *Phys. Rev. B* **2002**, *66*, 155125.
(84) Tkatchenko, A.; Scheffler, M. Accurate Molecular Van Der Waals Interactions from Ground-State Electron Density and Free-Atom Reference Data. *Phys. Rev. Lett.* **2009**, *102*, No. 073005.
(85) Barth, J. V.; Brune, H.; Ertl, G.; Behm, R. J. Scanning tunneling microscopy observations on the reconstructed Au(111) surface: Atomic structure, long-range superstructure, rotational domains, and surface defects. *Phys. Rev. B* **1990**, *42*, 9307−9318.
(86) Wegner, D.; Yamachika, R.; Wang, Y.; Brar, V. W.; Bartlett, B. M.; Long, J. R.; Crommie, M. F. Single-molecule charge transfer and bonding at an organic/inorganic interface: Tetracyanoethylene on noble metals. *Nano Lett.* **2008**, *8*, 131−135.
(87) Écija, D.; Otero, R.; Sánchez, L.; Gallego, J. M.; Wang, Y.; Alcamí, M.; Martín, F.; Martín, N.; Miranda, R. Crossover site-selectivity in the adsorption of the fullerene derivative PCBM on Au(111). *Angew. Chem., Int. Ed.* **2007**, *46*, 7874−7877.
(88) Monkhorst, H. J.; Pack, J. D. Special points for Brillouin-zone integrations. *Phys. Rev. B* **1976**, *13*, 5188−5192.
(89) Neugebauer, J.; Scheffler, M. Adsorbate-substrate and adsorbate-adsorbate interactions of Na and K adlayers on Al(111). *Phys. Rev. B* **1992**, *46*, 16067−16080.
(90) Duhm, S.; Gerlach, A.; Salzmann, I.; Bröker, B.; Johnson, R. L.; Schreiber, F.; Koch, N. PTCDA on Au(111), Ag(111) and Cu(111): Correlation of interface charge transfer to bonding distance. *Org. Electron.* **2008**, *9*, 111−118.
(91) Romaner, L.; Nabok, D.; Puschnig, P.; Zojer, E.; Ambrosch-Draxl, C. Theoretical study of PTCDA adsorbed on the coinage metal surfaces, Ag(111), Au(111) and Cu(111). *New J. Phys.* **2009**, *11*, No. 053010.

DOI: 10.1021/acsomega.9b02154
ACS Omega 2019, 4, 16906−16915

(92) Clark, S. J.; Segall, M. D.; Pickard, C. J.; Hasnip, P. J.; Probert, M. I. J.; Refson, K.; Payne, M. C. First principles methods using CASTEP. *Z. Kristallogr. - Cryst. Mater.* **2005**, *220*, 567.
(93) McNellis, E. R.; Meyer, J.; Reuter, K. Azobenzene at coinage metal surfaces: Role of dispersive van der Waals interactions. *Phys. Rev. B* **2009**, *80*, 205414.

DOI: 10.1021/acsomega.9b02154
ACS Omega 2019, 4, 16906−16915